Volume 10 | Number 17 | 7 May 2019 | Pages 4533–4716

Chemical Science

rsc.li/chemical-science

ISSN 2041-6539

ROYAL SOCIETY OF CHEMISTRY | Celebrating IYPT 2019

EDGE ARTICLE
Wendy L. Queen *et al.*
A new post-synthetic polymerization strategy makes metal–organic frameworks more stable

Chemical Science

EDGE ARTICLE

View Article Online
View Journal | View Issue

Cite this: *Chem. Sci.*, 2019, **10**, 4542

All publication charges for this article have been paid for by the Royal Society of Chemistry

Received 9th January 2019
Accepted 25th March 2019

DOI: 10.1039/c9sc00135b

rsc.li/chemical-science

A new post-synthetic polymerization strategy makes metal–organic frameworks more stable†

Shuliang Yang,‡[a] Li Peng,‡[a] Daniel T. Sun,[a] Mehrdad Asgari,[a] Emad Oveisi,[b] Olga Trukhina,[a] Safak Bulut,[a] Abbas Jamali[a] and Wendy L. Queen *[a]

Metal–organic frameworks are of interest in a number of host–guest applications. However, their weak coordination bonding often leads to instability in aqueous environments, particularly at extreme pH, and hence, is a challenging topic in the field. In this work, a two-step, post-synthetic polymerization method is used to create a series of highly hydrophobic, stable MOF composites. The MOFs are first coated with thin layers of polydopamine from free-base dopamine under a mild oxygen atmosphere, which then undergoes a Michael addition to covalently graft hydrophobic molecules to the external MOF surface. This easy, mild post-synthetic modification is shown to significantly improve the stability of a number of structurally diverse MOFs including HKUST-1 (Cu), ZIF-67 (Co), ZIF-8 (Zn), UiO-66 (Zr), Cu-TDPAT (Cu), Mg-MOF-74 (Mg) and MIL-100 (Fe) in wet, caustic (acidic and basic) environments as determined by powder X-ray diffraction and surface area measurements.

Introduction

Metal–organic frameworks (MOFs) have received tremendous attention due to unprecedented internal surface areas, tunable topologies, designable pore surfaces,[1–7] and their applicability in a number of energy related areas including catalysis, gas adsorption/separation, chemical sensing, energy storage/conversion and so on.[8–18] However, weak coordination bonding can limit the stability of some MOFs in water, particularly at extreme pH. To overcome this instability issue and expand the practical applications of the existing MOFs, two main methods have recently been developed.[19–29] One is to functionalize the organic linkers of unstable MOFs with hydrophobic functionality.[19–21] For example, Cohen *et al.* improved the hydrolytic stability of IRMOF-1, IRMOF-3 and MIL-53 through the introduction of hydrophobic alkyl groups such as isopropyl, isobutyl, and linear alkyl chains onto MOF ligands.[19] While this method can be highly effective one, the synthesis of the hydrophobic ligands and subsequently searching for the reaction conditions necessary to obtain a desired MOF can be in some instances time consuming. The second method is to introduce hydrophobic layers post synthetically onto the external MOF surface.[26–29] For example, Yu *et al.* reported a hydrophobic polydimethylsiloxane (PDMS) coating process, achieved by heating MOFs in the presence of a PDMS stamp in a sealed glass container at 235 °C.[30] In another study, Park *et al.* used calcination, 480 °C, to construct hydrophobic surfaces.[31] Though all of these reported methods are proven to be effective ways to improve the stability of some MOFs, it is still challenging to develop a general and mild way to functionalize various MOF surface to stabilize them under harsh conditions.

Given these challenges, we were inspired to design a new, mild process for hydrophobic surface functionalization that could be quickly applied to most MOFs. In nature, mussels firmly adhere to virtually all types of substrates under wet and harsh marine conditions through the secretion of an adhesive protein.[32,33] Similar to these proteins, polydopamine (PDA) has catechol and amine functionalities, which enable it to mimic the adhesive properties of mussel foot proteins.[34,35] Since 2007, PDA has been used as a platform for the functionalization of a wide number of material surfaces, even those with super hydrophobic surfaces.[32,36,37] However, to carry out the oxidative process required for dopamine polymerization, weakly alkaline, aqueous environments are required,[38–40] limiting the modification of water sensitive MOFs, such as HKUST-1, with PDA. In this work, we demonstrate that the use of free-base dopamine can promote polymerization under a mild oxygen atmosphere, eliminating the need for basic aqueous environments. This allows us to utilize PDA as an adhesive to attach highly hydrophobic perfluoro coatings onto the external surface of a set of structurally diverse MOFs, significantly improving their stability in acidic and/or basic aqueous environments. The two-step

[a]*Institute of Chemical Sciences and Engineering, École Polytechnique Fédérale de Lausanne (EPFL), CH-1051 Sion, Switzerland. E-mail: wendy.queen@epfl.ch; Tel: +41 216958243*

[b]*Interdisciplinary Center for Electron Microscopy, École Polytechnique Fédérale de Lausanne (EPFL), CH-1015 Lausanne, Switzerland*

† Electronic supplementary information (ESI) available: Detailed information for the synthesis and characterizations of all the materials. See DOI: 10.1039/c9sc00135b

‡ These authors have contributed equally to this study.

modification process is displayed in Fig. 1. First, free-base dopamine is synthesized and employed for polymerization onto the MOF surface. Next, is a fluorination step carried out *via* a Michael addition between 1*H*,1*H*,2*H*,2*H*-perfluorodecanethiol (HSF) and PDA (Fig. S1†).[41,42]

Results and discussion

Preparation and characterizations of MOF@PDA-SF composites

HKUST-1, also known as $Cu_3(BTC)_2$ (BTC^{3-} = benzene-1,3,5-tricarboxylate), is one of the most common MOFs studied for gas adsorption and catalysis, because it is easy to synthesize, cheap, and has open metal coordination sites.[43,44] However, HKUST-1 is unstable in water and humid atmospheres. Given this structural instability, HKUST-1 was chosen as the first example for the hydrophobic modification. Before the modification process, the HKUST-1 surface is smooth (Fig. 2a and d) and exhibits a light blue color (inset of Fig. 2a). After the PDA modification, the blue crystalline sample turns dark green, indicating the successful formation of HKUST-1@PDA (inset of Fig. 2b and h). Further, the polymer coating on the external MOF surface is clearly observed using both scanning electron microscope (SEM) and transmission electron microscopy (TEM) (Fig. 2b and e). SEM images reveal that the surface becomes rough, and powder X-ray diffraction (PXRD) shows that the crystal structure is well maintained after PDA introduction (Fig. 3a(III)). The Fourier-transform infrared spectroscopy (FT-IR) of HKUST-1@PDA shows the characteristic peaks belonging to the polymer (Fig. S2†). Further, high-resolution X-ray photoelectron spectroscopy (XPS) reveals that the Cu 2p spectrum of HKUST-1@PDA is very weak when compared to the parent MOF (Fig. S3†); this further confirms that the polymerization mainly occurs on the external surface, which obstructs the penetration of the X-rays into the MOF. Next, an HSF functionalization step is used to introduce hydrophobicity to the external MOF surface. The HSF reacts with the benzene ring of the PDA forming strong covalent bonds that inhibit leaching of the hydrophobic molecules from the MOF surface. Energy-dispersive X-ray spectroscopy in SEM (SEM-EDX) reveals that HKUST-1@PDA-SF consists of Cu, C, O, N, F and S (Fig. S4†), and PXRD patterns confirm the MOF structure again retains its crystallinity after the fluorination step (Fig. 3a(IV)). SEM and TEM images (Fig. 2c and f) confirm that the polymer layer is present on the surface after HSF addition. Meanwhile the green color of the crystalline sample is still maintained (Fig. 2i). Also, SEM reveals the presence of nano-papillae, which make the surface rough. It should be noted that this kind of binary structure is similarly observed on the surface of the lotus-leaf, which aids in repelling water.[45] FT-IR spectrum of HKUST-1@PDA-SF shows vibrational bands at 1150 and 1206 cm^{-1}, which are assigned to the symmetric and asymmetric $-CF_2-$ stretches, respectively (Fig. S2†).[46] Moreover, a solid-state ^{19}F magic angle spinning nuclear magnetic resonance (MAS NMR) spectrum of HKUST-1@PDA-SF confirms the successful grafting of the hydrophobic HSF molecules onto the MOF surface (Fig. S5†). It should be noted that the Brunauer–Emmett–Teller (BET) surface area of HKUST-1@PDA-SF composite is reduced from 1843 to 1286 $m^2\ g^{-1}$, due to the 16.2 wt% loading of the dense polymer in the modified MOF composite (Fig. 3b and S6†). Given the significant reduction in surface area on our first attempt, the post-synthetic treatment was later optimized in order to obtain higher porosity all while maintaining high composite stability (Fig. S7†). At a PDA-SF loading of 6.8 wt% (named as HKUST-1@PDA-SF-2), the surface area is only reduced to 1600 $m^2\ g^{-1}$ after the appendage of the HSF molecules.

To further determine the location of PDA-SF in the HKUST-1@PDA-SF composite, various elemental maps were obtained *via* EDX elemental mapping in scanning TEM mode (STEM-EDX). Fig. 4 reveals that the PDA-SF polymer composite contains N, F and S on the external surface of HKUST-1. However, given the possible diffusion of the free-base dopamine precursor into HKUST-1, small amounts of polymer could also be present inside the MOF. It is expected that if dopamine diffuses into the framework that it will readily bind Cu(II), blocking the open metal sites on the internal MOF surface. As such, *in situ* diffuse reflectance infrared Fourier transform

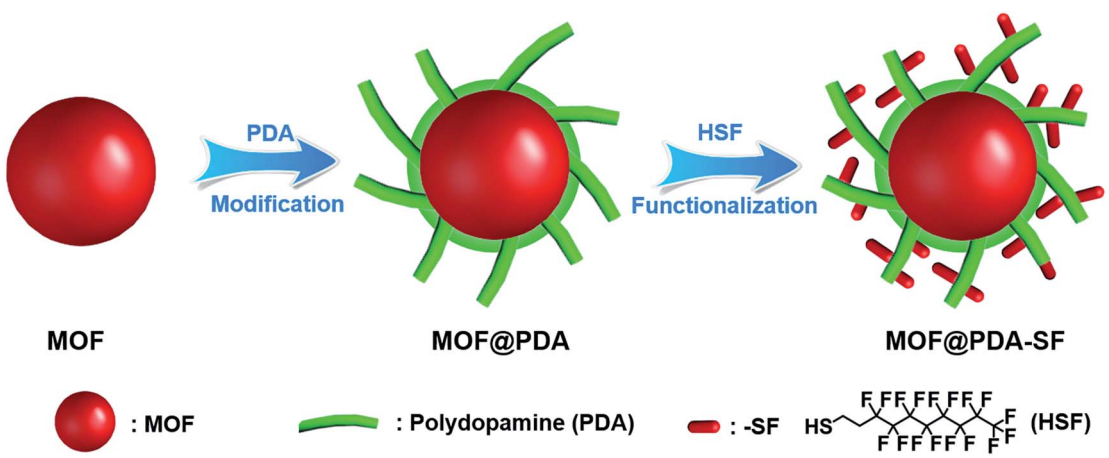

Fig. 1 The modification process used to prepare hydrophobic MOF@PDA-SF composites.

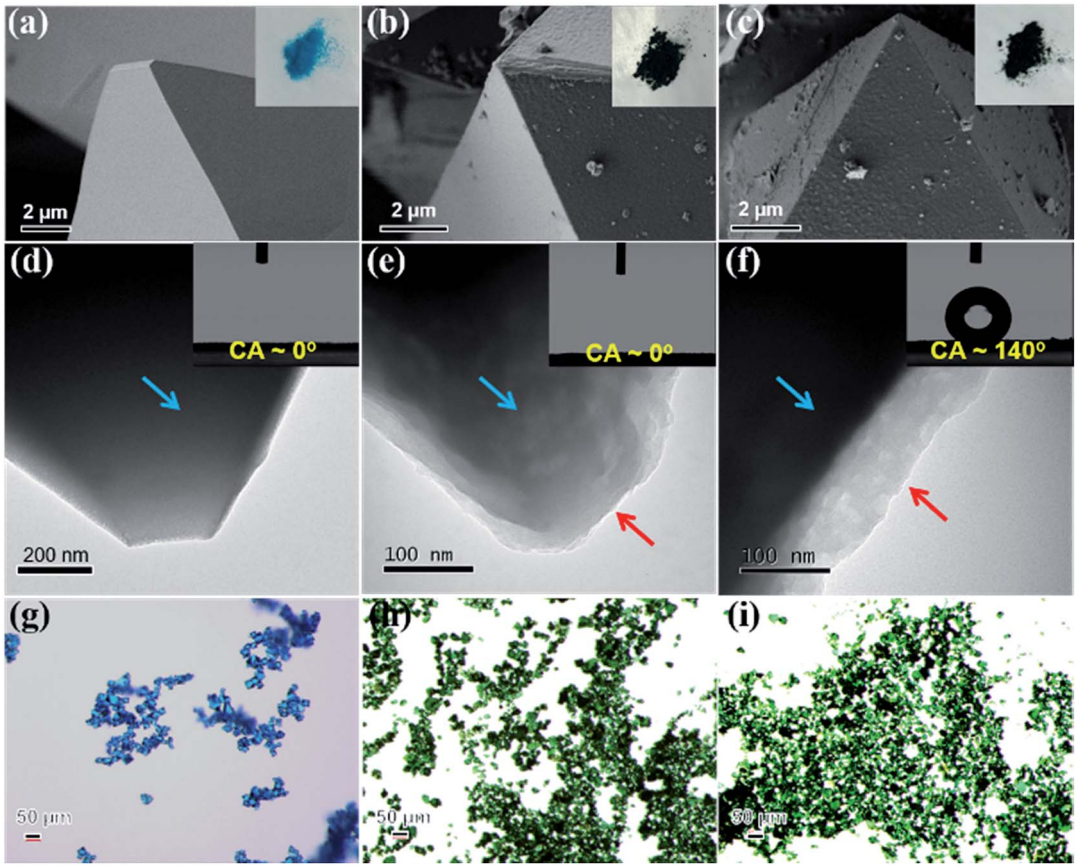

Fig. 2 SEM, TEM and light microscope images of HKUST-1 (a, d, g), HKUST-1@PDA (b, e, h) and HKUST-1@PDA-SF (c, f, i). The insets are the photograph and water contact angle (CA) of the corresponding samples. TEM images show that the MOF (blue arrow) are coated with a uniform polymer layer (red arrow).

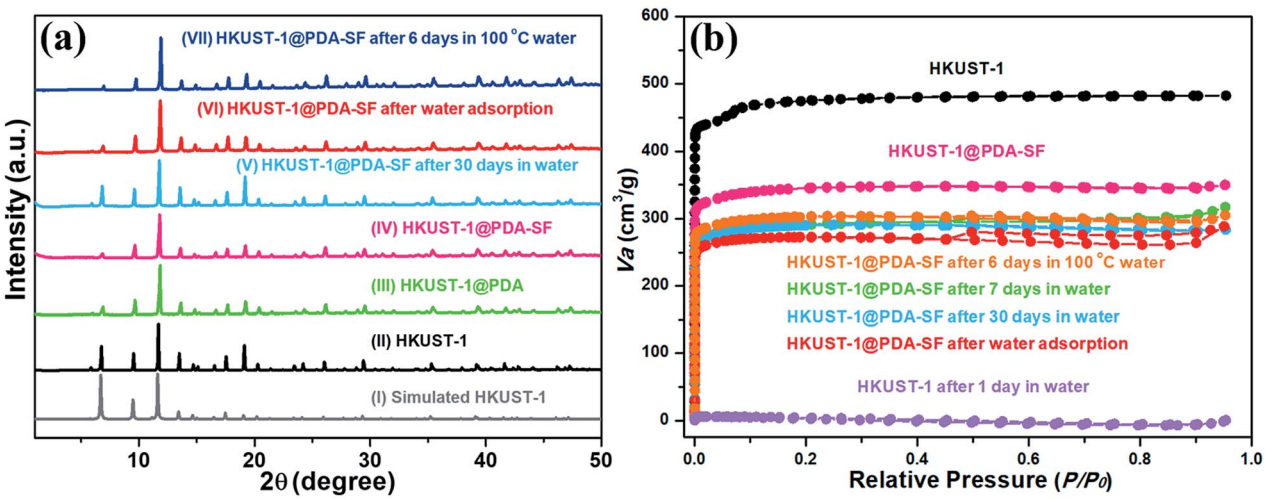

Fig. 3 XRD patterns (a) and N_2 adsorption–desorption isotherms (b) of the unmodified HKUST-1 and the corresponding modified samples. The surface areas of samples are: as-synthesized HKUST-1 (black, 1843 $m^2\ g^{-1}$), HKUST-1@PDA-SF (pink, 1286 $m^2\ g^{-1}$), HKUST-1@PDA-SF after 6 days in 100 °C water (orange, 1211 $m^2\ g^{-1}$), HKUST-1@PDA-SF after 7 days in water (green, 1153 $m^2\ g^{-1}$), HKUST-1@PDA-SF after 30 days in water (cyan, 1186 $m^2\ g^{-1}$), HKUST-1@PDA-SF after water adsorption 2 runs (red, 1093 $m^2\ g^{-1}$) and HKUST-1 after 1 day in water (purple, 255 $m^2\ g^{-1}$).

spectroscopy (*in situ* DRIFTs) was used to probe the material for open Cu(II) sites. The sample was activated and dosed with CO. The spectra showed the characteristic peak of Cu(II)-bound CO of ~2176 cm^{-1}, a value that is significantly shifted from the expected stretching frequency of free CO, 2143 cm^{-1}. This implies that if a small amount of PDA-SF has diffused inside,

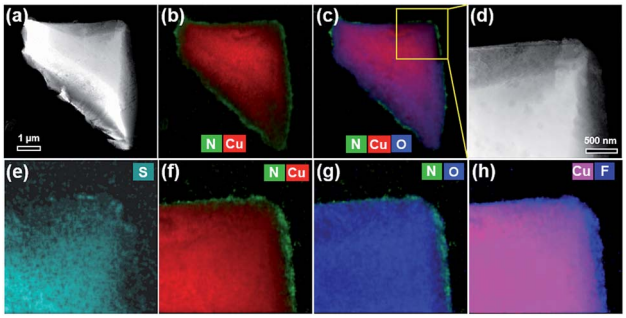

Fig. 4 High-angle annular dark field scanning TEM (HAADF-STEM) imaging (a, d) and corresponding EDX elemental maps (b and c, e–h).

there is still a large number of open metal sites (Fig. S8†).[47,48] It should be pointed out that if free-base dopamine diffuses inside HKUST-1, it could partially shield the Cu^{2+} sites. Hence, the likelihood of possible attack from the H_2O molecules can be reduced, further improving the MOF's water stability.[49]

Stability test and application

To explore the efficiency of our method to improve MOF stability, both pristine HKUST-1 and HKUST-1@PDA-SF samples were immersed in water. HKUST-1 expectedly degraded in less than two hours (Fig. S9a†), and PXRD and SEM of the recovered sample confirm a change in the crystal structure and morphology (Fig. S9b and c†). Interestingly, however, the PXRD of the HKUST-1@PDA-SF composite shows that the MOF is well-maintained with no sign of a structural transition after immersion for over 30 days (Fig. 3a(V)). Further, the surface area only shows a very small amount of loss from 1286 to 1186 $m^2\ g^{-1}$ (Fig. 3b) over this period. It should be noted that to date, under the conditions we have tested, the decomposition or structural transitions of HKUST-1 with the hydrophobic coating has not yet occurred. The test conditions include the aforementioned immersion, boiling the material at 100 °C for six days, and also placing the composite in highly acid or basic conditions (pH = ~2 or 12) for one day (Fig. 3a(VII), b and S10†). HKUST-1@PDA-SF-2 also exhibits the same stability as the aforementioned composite with 16.2 wt% PDA-SF (Fig. S7† and Table 1). Next, several H_2O adsorption/desorption isotherms were obtained from the parent MOF and its corresponding composite. While the parent MOF loses a large percentage of its water sorption capacity after each successive adsorption/desorption cycle due to its high instability in the presence of water vapor,[23,50,51] HKUST-1@PDA-SF has no sign of degradation, even with cycling (Fig. 3a(VI) and S11†). Despite the hydrophobic nature of the MOF composite, the water adsorption profile does not change, and the capacity is only reduced by 25% from 0.6 g H_2O/g for HKUST-1 to 0.45 g H_2O/g for HKUST-1@PDA-SF. The decrease in water capacity after the post-synthetic modification correlates well with the aforementioned decrease in surface area. Further, it is noted that the equilibration time required for water adsorption in the composite is significantly longer than that of the parent MOF; this implies that the surface coating slows the rate at which water is able to diffuse into the structure. To further give evidence of this, the MOF and its corresponding composite were activated at 125 °C for 12 hours to remove all residual solvents. Then, both materials were exposed to air with 34% relative humidity for 3 minutes. Subsequently, CO_2 adsorption isotherms were collected on the unactivated samples. It is noted that while the CO_2 adsorption capacity of the HKUST-1 is decreased by 29.8%, the capacity of HKUST-1@PDA-SF is only decreased by 3.6% at 0.15 bar, which is the partial pressures of CO_2 in post-combustion flue gas (Fig. S12†).

Given the high hydrophobicity (with a water contact angle of 140°), slowed water permeability, and unprecedented stability of HKUST-1@PDA-SF, this new surface modification offers an opportunity to, for the first time, demonstrate the applicability of HKUST-1 in a number of water-containing separations. For example, currently there is a high demand for offshore oil production, which lends to frequent oil spills, and the chemical industry employs a number of organic compounds in various processes that are too often mistakenly discharged into the water supply. With this awareness, materials able to promote oil/water separations are becoming increasingly important.[52–54] As such, we attempted to carry out the separation of chloroform/H_2O, hexane/H_2O, toluene/H_2O and gasoline/H_2O as a proof-of-concept for oil and water separations. For this, a home-made separator was designed (see ESI†). Because HKUST-1 is not water- or oil-repellant, it permits both to permeate through and of course also readily degrades (Fig. S9 and S13a†). However, for HKUST-1@PDA-SF, the water sits on top of the material while chloroform, hexane, toluene and gasoline readily pass (Fig. S13b†). Like the aforementioned water adsorption isotherms, these separations demonstrate that the hydrophobic coating has significantly slowed water permeation. It is also noted that after the separation, the crystal structure of the recovered HKUST-1@PDA-SF is well-maintained (Fig. S14†). Considering the tunable pore size and functionality in MOFs, it is thought that this modification method has great potential to employ many MOFs in a host of gas and liquid separations that were not before accessible.

Extension of the current strategy in other MOFs

Encouraged by the results with HKUST-1, we extended this coating method to a selected set of structurally diverse MOFs including ZIF-67, ZIF-8, UiO-66, Mg-MOF-74, MIL-100 (Fe), and Cu-TDPAT.[55–58] While the chosen materials have reported water stability at room temperature, the idea was to see if the coating could improve their stability under more harsh conditions, in both highly acidic and basic media. First, ZIF-67 nanocubes (1466 $m^2\ g^{-1}$) were prepared,[59] followed by the corresponding composite, ZIF-67@PDA-SF, which contained a 16.8 wt% PDA-SF loading. From the SEM images, it can be seen that the nanocube morphology is well maintained after the modification (Fig. 5b) and the water CA increases from 67° to 147° (insets of Fig. 5a and b). While the surface area of the composite is decreased after the post-synthetic modification (to 683 $m^2\ g^{-1}$) (Fig. S15a†), the CO_2 adsorption capacity was significantly enhanced by ~30% at 1 bar (Fig. S15b†). The latter is likely due

Table 1 Comparison of the properties and stabilities of the parent MOFs and their corresponding MOF-composites soaked under highly acidic or basic conditions for 24 hours. Ticks mean stable and crosses mean unstable

Sample name/formula	BET surface area ($m^2\ g^{-1}$)	Contact angle (°)	Polymer loading (wt%)	H_2SO_4 treatment, pH = 0, 1, 2 or 3 for 24 h	BET surface area after H_2SO_4 treatment ($m^2\ g^{-1}$)	NaOH treatment, pH = 11, 12 or 13 for 24 h	BET surface area after NaOH treatment ($m^2\ g^{-1}$)
HKUST-1 $Cu_3(BTC)_2$, BTC^{3-} = benzene-1,3,5-tricarboxylate	1843	~0	—	×	—	×	—
HKUST-1@PDA-SF	1286	140	16.2	✓	1247	✓	1242
HKUST-1@PDA-SF-2	1600	135	6.8	✓	1586	✓	1571
ZIF-67 $Co(MIm)_2$, MIm = 2-methylimidazolate	1466	67	—	×	—	×	—
ZIF-67@PDA-SF	683	147	16.8	✓	729	✓	738
ZIF-67@PDA-SF-2	1312	139	11.5	✓	1303	✓	1293
ZIF-8 $Zn(MIm)_2$, MIm = 2-methylimidazolate	1788	~0	—	×	—	✓	1710
ZIF-8@PDA-SF	1389	149	7.6	✓	1387	✓	1411
Mg-MOF-74 $Mg_2(dobdc)$, $dobdc^{4-}$ = 2,5-dioxido-1,4-benzenedicarboxylate	1182	~0	—	×	—	✓	1138
Mg-MOF-74@PDA-SF	918	138	12.8	✓	867	✓	952
MIL-100-Fe $Fe_3(BTC)_2$, BTC^{3-} = benzene-1,3,5-tricarboxylate	1587	~0	—	×	—	✓	1579
MIL-100-Fe@PDA-SF	1266	127	14.7	✓	1369	✓	1262
UiO-66 $Zr_6O_4(OH)_4(BDC)_6$, BDC^{2-} = 1,4-dicarboxybenzene	1430	~0	—	×	—	×	—
UiO-66@PDA-SF	638	141	10.3	✓	626	✓	581
Cu-TDPAT $Cu_3(TDPAT)$, TDPAT = 2,4,6-tris(3,5 dicarboxylic phenylamino)-1,3,5-triazine	2254	~0	—	×	—	×	—
Cu-TDPAT@PDA-SF	1835	146	12.5	✓	1784	✓	1778

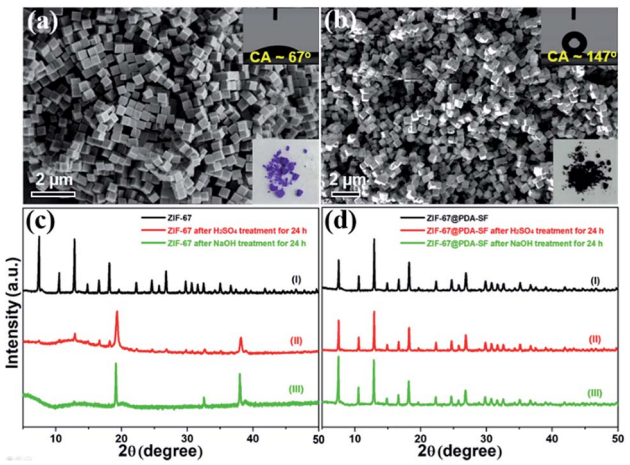

Fig. 5 SEM images of ZIF-67 nanocubes (a), hydrophobically modified ZIF-67@PDA-SF (b), and XRD patterns of ZIF-67 and ZIF-67@PDA-SF after exposure to H_2SO_4 (pH = 3)/NaOH (pH = 13) solution for 24 h (c and d). The insets are the water contact angles (CA) and a photograph of ZIF-67 (a) and ZIF-67@PDA-SF (b), respectively.

to new interactions between the CO_2 and the nitrogen species found in PDA and strongly polarizing C–F species in the perfluoro coating.[60,61] To test the improved stability of ZIF-67@PDA-SF (contact angle: 147°), the parent MOF and composite were soaked in an aqueous H_2SO_4 (pH = 3) and NaOH solution (pH = 13). While the parent structure completely degrades in either solution, as indicated by the XRD pattern and SEM images (Fig. 5c(ii, iii) and S16a, b†), ZIF-67@PDA-SF remains after 24 h with no obvious sign of degradation (Fig. 5d(ii, iii) and S16c, d†). Further, surface area analysis (Fig. S17†) of the composite indicates no significant change in the BET surface area from the parent composite, 683 $m^2\ g^{-1}$, to the acid and base treated composite, 729 $m^2\ g^{-1}$ and 738 $m^2\ g^{-1}$, respectively. These results give a good indication that the coating method indeed enhances the stability of this MOF in harsh conditions.

As in the case of HKUST-1, we also demonstrated that reducing the quantity of PDA-SF could enhance the porosity of the resulting composite all while still maintaining high stability. For this, a second composite, ZIF-67@PDA-SF-2, was prepared. The percentage of PDA-SF, 11.5 wt%, is significantly lower than the original composite ZIF-67@PDA-SF that contains 16.8 wt% PDA-SF. After the surface appendage of HSF molecules, the surface area of ZIF-67@PDA-SF-2 is determined to be 1312 $m^2\ g^{-1}$, which is significantly higher than ZIF-67@PDA-SF, 683 $m^2\ g^{-1}$ (Table 1). Further, the stability was again assessed in highly acidic and basic conditions for 24 hours, and the same results are obtained as previously observed for ZIF-67@PDA-SF (Fig. S18,† Table 1).

Next, using similar procedures, hydrophobic composites of ZIF-8, UiO-66, Cu-TDPAT, Mg-MOF-74, and MIL-100-Fe were prepared. As in the previous cases with HKUST-1 and ZIF-67, the surface polymer layer is clearly observed *via* TEM and the

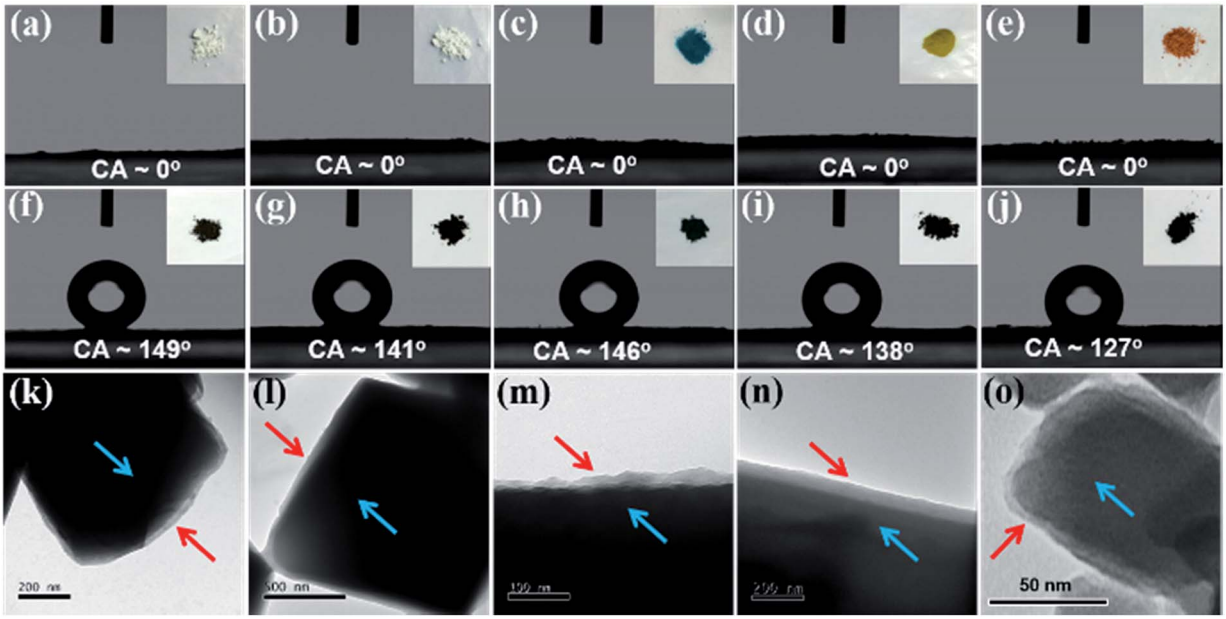

Fig. 6 The water contact angle of the unmodified samples including ZIF-8 (a), UiO-66 (b), Cu-TDPAT (c), Mg-MOF-74 (d), MIL-100-Fe (e) and the contact angle of the corresponding PDA-SF modified samples ZIF-8@PDA-SF (f), UiO-66@PDA-SF (g), Cu-TDPAT@PDA-SF (h), Mg-MOF-74@PDA-SF (i), MIL-100-Fe@PDA-SF (j). The insets are the photographs of unmodified samples (a–f) and modified samples (g–l). TEM images of the corresponding modified samples ZIF-8@PDA-SF (k), UiO-66@PDA-SF (l), Cu-TDPAT@PDA-SF (m), Mg-MOF-74@PDA-SF (n), MIL-100-Fe@PDA-SF (o). TEM images show that the MOF (blue arrow) are coated with a uniform polymer layer (red arrow).

structures of the parent materials are well maintained after the modification (Fig. 6 and S19, S20†). The hydrophobic coating increases the water contact angles (CA) from ~0° for all parent MOF structures to 149°, 141°, 146°, 138°, and 127°, for ZIF-8@PDA-SF, UiO-66@PDA-SF, Cu-TDPAT@PDA-SF, Mg-MOF-74@PDA-SF, and MIL-100-Fe@PDA-SF, respectively. Several of the contact angles are approaching super-hydrophobic, >150°. As such, water droplets readily roll off the surface of ZIF-8@PDA-SF during the CA experiment (ESI Video S1†). Further, all of these composites exhibit high stability in either acidic or basic conditions, while the parent MOFs are shown to decompose. XRD patterns and surface area analysis, collected after soaking the composite materials in acidic (pH = 0–3) or basic solutions (pH = 11–13) for 24 hours indicate minimal to no change after exposure to these harsh conditions (Fig. S21† and Table 1). These data strongly suggest that this simple method is an effective, universal way to introduce hydrophobicity to MOFs and improve stability.

For the Mg-MOF-74 composite, the hydrophobicity is easily tuned by introducing varying amounts of free-base dopamine and HSF. For example, the contact angle increased from 100 to 138° through the addition of more free-base dopamine and HSF during the post-synthetic modification of Mg-MOF-74 (Fig. S22†). Considering the tunable porosity and hydrophobicity of the resulting composites and several experiments that suggest that water vapor diffusion into HKUST-1 is slowed in the presence of the hydrophobic coating, it is hypothesized that optimizing the surface coating process can lend to enhanced performance of various MOFs in humid gas separations. Further, considering that PDA and other redox active polymers are able to readily reduce metal ions and that previous studies have shown that catalytic activity and selectivity can be enhanced after surface functionalization with hydrophilic-hydrophobic entities,[62,63] these novel MOF composites provoke interest for future catalytic studies.

Conclusions

In summary, a facile mussel-inspired modification method was developed enabling the introduction of highly hydrophobic coatings onto a number of structurally diverse MOFs. This novel technique, which entails the use of free-base dopamine to graft hydrophobic HSF molecules onto the external MOF surface, significantly enhances MOF stability in water and in acidic or basic conditions. Free-base dopamine was selected as a binder between the MOF and HSF because it is a strong adhesive and polymerizes under a mild oxygen atmosphere at room temperature making it suitable to modify even the most unstable MOFs. Employing the free base form eliminates the need for basic aqueous environments that are required when using dopamine hydrochloride. Also, all the MOF composites are rapidly accessible, eliminating the need for other time consuming efforts focused on, for instance, designing new hydrophobic ligands to improve MOF stability.

As a proof-of-concept, HKUST-1@PDA-SF is shown for the first time to be recyclable with water adsorption/desorption and stable in boiling water and acidic or basic aqueous media for extended periods of time. Given the added water stability combined with significantly slowed water permeability, HKUST-1@PDA-SF is also shown applicable in oil/water separations.

Last, the method was applied to a number of other composites using a structurally diverse set of MOFs with varying

metals, ligands, and topologies. The as-prepared composites, including ZIF-67@PDA-SF, ZIF-8@PDA-SF, UiO-66@PDA-SF, Cu-TDPAT@PDA-SF, Mg-MOF-74@PDA-SF, and MIL-100-Fe@PDA-SF, show excellent stability even under harsh acid or basic conditions. Considering the novel results obtained from HKUST-1 and the many other structurally dissimilar frameworks, it is thought that this facile, mild method can be universally applied to improve the stability most MOFs and any other materials known to have water/pH instability. It is expected that this work can open doors to numerous new applications that were before inaccessible, and/or enhance MOF performance in existing areas coupled to catalysis, selective gas separation, delivery *etc* by inhibiting decomposition, enhancing hydrophobicity and decreasing water permeability.

Conflicts of interest

There are no conflicts to declare.

Acknowledgements

This work was supported by the Swiss National Science Foundation under grant PYAPP2_160581. M. A. is financially supported by the Swiss Commission for Technology and Innovation (CTI). O. T. is financially supported by the National Center for Competence in Research (NCCR) "Materials' Revolution: Computational Design and Discovery of Novel Materials (MARVEL)" of the Swiss National Science Foundation (SNSF) and EPFL Fellows co-funded by Marie Skłodowska-Curie. The authors thank Jacques Morisod for help with the contact angle test.

Notes and references

1 H. Furukawa, K. E. Cordova, M. O'Keeffe and O. M. Yaghi, *Science*, 2013, **341**, 1230444.
2 J. E. Mondloch, M. J. Katz, W. C. Isley III, P. Ghosh, P. Liao, W. Bury, G. W. Wagner, M. G. Hall, J. B. DeCoste, G. W. Peterson, R. Q. Snurr, C. J. Cramer, J. T. Hupp and O. K. Farha, *Nat. Mater.*, 2015, **14**, 512–516.
3 L. Sun, M. G. Campbell and M. Dincă, *Angew. Chem., Int. Ed.*, 2016, **55**, 3566–3579.
4 L. Zou, D. Feng, T.-F. Liu, Y.-P. Chen, S. Yuan, K. Wang, X. Wang, S. Fordham and H.-C. Zhou, *Chem. Sci.*, 2016, **7**, 1063–1069.
5 S. Kitagawa, R. Kitaura and S.-i. Noro, *Angew. Chem., Int. Ed.*, 2004, **43**, 2334–2375.
6 C. Wang, Z. Xie, K. E. deKrafft and W. Lin, *J. Am. Chem. Soc.*, 2011, **133**, 13445–13454.
7 G. Férey, C. Serre, C. Mellot-Draznieks, F. Millange, S. Surblé, J. Dutour and I. Margiolaki, *Angew. Chem., Int. Ed.*, 2004, **43**, 6296–6301.
8 J. Lee, O. K. Farha, J. Roberts, K. A. Scheidt, S. T. Nguyen and J. T. Hupp, *Chem. Soc. Rev.*, 2009, **38**, 1450–1459.
9 J. Yang, F. Zhang, H. Lu, X. Hong, H. Jiang, Y. Wu and Y. Li, *Angew. Chem., Int. Ed.*, 2015, **54**, 10889–10893.
10 L. Peng, J. Zhang, Z. Xue, B. Han, X. Sang, C. Liu and G. Yang, *Nat. Commun.*, 2014, **5**, 5465.
11 Y. Liu, J. H. Pan, N. Wang, F. Steinbach, X. Liu and J. Caro, *Angew. Chem., Int. Ed.*, 2015, **54**, 3028–3032.
12 X. Han, H. G. W. Godfrey, L. Briggs, A. J. Davies, Y. Cheng, L. L. Daemen, A. M. Sheveleva, F. Tuna, E. J. L. McInnes, J. Sun, C. Drathen, M. W. George, A. J. Ramirez-Cuesta, K. M. Thomas, S. Yang and M. Schröder, *Nat. Mater.*, 2018, **17**, 691–696.
13 Q.-L. Zhu, J. Li and Q. Xu, *J. Am. Chem. Soc.*, 2013, **135**, 10210–10213.
14 M. G. Campbell, S. F. Liu, T. M. Swager and M. Dincă, *J. Am. Chem. Soc.*, 2015, **137**, 13780–13783.
15 I. Stassen, N. Burtch, A. Talin, P. Falcaro, M. Allendorf and R. Ameloot, *Chem. Soc. Rev.*, 2017, **46**, 3185–3241.
16 X. Sang, J. Zhang, J. Xiang, J. Cui, L. Zheng, J. Zhang, Z. Wu, Z. Li, G. Mo, Y. Xu, J. Song, C. Liu, X. Tan, T. Luo, B. Zhang and B. Han, *Nat. Commun.*, 2017, **8**, 175.
17 A. M. Wright, Z. Wu, G. Zhang, J. L. Mancuso, R. J. Comito, R. W. Day, C. H. Hendon, J. T. Miller and M. Dincă, *Chem*, 2018, **4**, 2894–2901.
18 P. Hu, X. Liang, M. Yaseen, X. Sun, Z. Tong, Z. Zhao and Z. Zhao, *Chem. Eng. J.*, 2018, **332**, 608–618.
19 J. G. Nguyen and S. M. Cohen, *J. Am. Chem. Soc.*, 2010, **132**, 4560–4561.
20 S. Mukherjee, A. M. Kansara, D. Saha, R. Gonnade, D. Mullangi, B. Manna, A. V. Desai, S. H. Thorat, P. S. Singh, A. Mukherjee and S. K. Ghosh, *Chem.–Eur. J.*, 2016, **22**, 10937–10943.
21 Q. Sun, H. He, W.-Y. Gao, B. Aguila, L. Wojtas, Z. Dai, J. Li, Y.-S. Chen, F.-S. Xiao and S. Ma, *Nat. Commun.*, 2016, **7**, 13300.
22 T. Wu, L. Shen, M. Luebbers, C. Hu, Q. Chen, Z. Ni and R. I. Masel, *Chem. Commun.*, 2010, **46**, 6120.
23 A. Carné-Sánchez, K. C. Stylianou, C. Carbonell, M. Naderi, I. Imaz and D. Maspoch, *Adv. Mater.*, 2015, **27**, 869–873.
24 S. He, H. Wang, C. Zhang, S. Zhang, Y. Yu, Y. Lee and T. Li, *Chem. Sci.*, 2019, **10**, 1816–1822.
25 J. B. Decoste, G. W. Peterson, M. W. Smith, C. A. Stone and C. R. Willis, *J. Am. Chem. Soc.*, 2012, **134**, 1486–1489.
26 J. Castells-Gil, F. Novio, N. M. Padial, S. Tatay, D. Ruíz-Molina and C. Martí-Gastaldo, *ACS Appl. Mater. Interfaces*, 2017, **9**, 44641–44648.
27 J. B. DeCoste, J. M. S. Denny, G. W. Peterson, J. J. Mahle and S. M. Cohen, *Chem. Sci.*, 2016, **7**, 2711–2716.
28 Y. Chen, S. Li, X. Pei, J. Zhou, X. Feng, S. Zhang, Y. Cheng, H. Li, R. Han and B. Wang, *Angew. Chem., Int. Ed.*, 2016, **55**, 3419–3423.
29 X. Qian, F. Sun, J. Sun, H. Wu, F. Xiao, X. Wu and G. Zhu, *Nanoscale*, 2017, **9**, 2003–2008.
30 W. Zhang, Y. Hu, J. Ge, H.-L. Jiang and S.-H. Yu, *J. Am. Chem. Soc.*, 2014, **136**, 16978–16981.
31 S. J. Yang and C. R. Park, *Adv. Mater.*, 2012, **24**, 4010–4013.
32 H. Lee, S. M. Dellatore, W. M. Miller and P. B. Messersmith, *Science*, 2007, **318**, 426–430.
33 Y. Liu, K. Ai and L. Lu, *Chem. Rev.*, 2014, **114**, 5057–5115.

34 Q. Wei, K. Achazi, H. Liebe, A. Schulz, P. L. Noeske, I. Grunwald and R. Haag, *Angew. Chem., Int. Ed.*, 2014, **53**, 11650–11655.
35 Z.-X. Wang, C.-H. Lau, N.-Q. Zhang, Y.-P. Bai and L. Shao, *J. Mater. Chem. A*, 2015, **3**, 2650–2657.
36 J. Jiang, L. Zhu, L. Zhu, B. Zhu and Y. Xu, *Langmuir*, 2011, **27**, 14180–14187.
37 C. Zhang, L. Gong, L. Xiang, Y. Du, W. Hu, H. Zeng and Z.-K. Xu, *ACS Appl. Mater. Interfaces*, 2017, **9**, 30943–30950.
38 F.-X. Ma, H. B. Wu, B. Y. Xia, C.-Y. Xu and X. W. D. Lou, *Angew. Chem., Int. Ed.*, 2015, **54**, 15395–15399.
39 C. Zhang, Y. Ou, W.-X. Lei, L.-S. Wan, J. Ji and Z.-K. Xu, *Angew. Chem., Int. Ed.*, 2016, **55**, 3054–3057.
40 Y. Lv, C. Zhang, A. He, S.-J. Yang, G.-P. Wu, S. B. Darling and Z.-K. Xu, *Adv. Funct. Mater.*, 2017, **27**, 1700251.
41 C. Ruan, K. Ai, X. Li and L. Lu, *Angew. Chem., Int. Ed.*, 2014, **53**, 5556–5560.
42 X. Yu, Q.-Z. Zhong, H.-C. Yang, L.-S. Wan and Z.-K. Xu, *J. Phys. Chem. C*, 2015, **119**, 3667–3673.
43 Z. Wang and Q. Chen, *Green Chem.*, 2016, **18**, 5884–5889.
44 J. L. C. Rowsell and O. M. Yaghi, *J. Am. Chem. Soc.*, 2006, **128**, 1304–1315.
45 Q. Xie, J. Xu, L. Feng, L. Jiang, W. Tang, X. Luo and C. C. Han, *Adv. Mater.*, 2004, **16**, 302–305.
46 Y. Zhu, D. Hu, M. X. Wan, L. Jiang and Y. Wei, *Adv. Mater.*, 2007, **19**, 2092–2096.
47 C. Prestipino, L. Regli, J. G. Vitillo, F. Bonino, A. Damin, C. Lamberti, A. Zecchina, P. L. Solari, K. O. Kongshaug and S. Bordiga, *Chem. Mater.*, 2006, **18**, 1337–1346.
48 E. D. Bloch, M. R. Hudson, J. A. Mason, S. Chavan, V. Crocellà, J. D. Howe, K. Lee, A. L. Dzubak, W. L. Queen, J. M. Zadrozny, S. J. Geier, L.-C. Lin, L. Gagliardi, B. Smit, J. B. Neaton, S. Bordiga, C. M. Brown and J. R. Long, *J. Am. Chem. Soc.*, 2014, **136**, 10752–10761.
49 L. N. McHugh, M. J. McPherson, L. J. McCormick, S. A. Morris, P. S. Wheatley, S. J. Teat, D. McKay, D. M. Dawson, C. E. F. Sansome, S. E. Ashbrook, C. A. Stone, M. W. Smith and R. E. Morris, *Nat. Chem.*, 2018, **10**, 1096–1102.
50 J. Canivet, A. Fateeva, Y. Guo, B. Coasne and D. Farrusseng, *Chem. Soc. Rev.*, 2014, **43**, 5594–5617.
51 H. Furukawa, F. Gándara, Y.-B. Zhang, J. Jiang, W. L. Queen, M. R. Hudson and O. M. Yaghi, *J. Am. Chem. Soc.*, 2014, **136**, 4369–4381.
52 J. Ge, L.-A. Shi, Y.-C. Wang, H.-Y. Zhao, H.-B. Yao, Y.-B. Zhu, Y. Zhang, H.-W. Zhu, H.-A. Wu and S.-H. Yu, *Nat. Nanotechnol.*, 2017, **12**, 434.
53 M. Zhang, X. Xin, Z. Xiao, R. Wang, L. Zhang and D. Sun, *J. Mater. Chem. A*, 2017, **5**, 1168–1175.
54 Y. Sun, Q. Sun, H. Huang, B. Aguila, Z. Niu, J. A. Perman and S. Ma, *J. Mater. Chem. A*, 2017, **5**, 18770–18776.
55 R. Luebke, J. F. Eubank, A. J. Cairns, Y. Belmabkhout, L. Wojtas and M. Eddaoudi, *Chem. Commun.*, 2012, **48**, 1455–1457.
56 J. H. Cavka, S. Jakobsen, U. Olsbye, N. Guillou, C. Lamberti, S. Bordiga and K. P. Lillerud, *J. Am. Chem. Soc.*, 2008, **130**, 13850–13851.
57 L.-C. Lin, J. Kim, X. Kong, E. Scott, T. M. McDonald, J. R. Long, J. A. Reimer and B. Smit, *Angew. Chem., Int. Ed.*, 2013, **52**, 4410–4413.
58 A. Phan, C. J. Doonan, F. J. Uribe-Romo, C. B. Knobler, M. O'Keeffe and O. M. Yaghi, *Acc. Chem. Res.*, 2010, **43**, 58–67.
59 H. Hu, B. Y. Guan and X. W. Lou, *Chem*, 2016, **1**, 102–113.
60 Y. Zhao, K. X. Yao, B. Teng, T. Zhang and Y. Han, *Energy Environ. Sci.*, 2013, **6**, 3684–3692.
61 L. Peng, S. Yang, D. T. Sun, M. Asgari and W. L. Queen, *Chem. Commun.*, 2018, **54**, 10602–10605.
62 D. T. Sun, N. Gasilova, S. Yang, E. Oveisi and W. L. Queen, *J. Am. Chem. Soc.*, 2018, **140**, 16697–16703.
63 G. Huang, Q. Yang, Q. Xu, S.-H. Yu and H.-L. Jiang, *Angew. Chem., Int. Ed.*, 2016, **55**, 7379–7383.